Role of Solution Structure in Self-Assembly of Conjugated Block Copolymer Thin Films

Michael A. Brady,[§] Sung-Yu Ku,[§] Louis A. Perez,[§] Justin E. Cochran,[♯] Kristin Schmidt,[§] Thomas M. Weiss,[†] Michael F. Toney,[†] Harald Ade,[□] Alexander Hexemer,[||] Cheng Wang,[||] Craig J. Hawker,[§,♯] Edward J. Kramer,[§,‡,∩] Michael L. Chabinyc[,§]*

[§]Materials Department, [♯]Department of Chemistry & Biochemistry, [‡]Department of Chemical Engineering, University of California, Santa Barbara, CA 93106, U.S.A.

[†]Stanford Synchrotron Radiation Lightsource, SLAC National Accelerator Laboratory, Menlo Park, CA 94025, U.S.A.

[□]Department of Physics, North Carolina State University, Raleigh, NC 27695, U.S.A.

[||]Advanced Light Source, Lawrence Berkeley National Laboratory, Berkeley, CA 94720, U.S.A.

ABSTRACT: Conjugated block copolymers provide a pathway to achieve thermally stable nanostructured thin films for organic solar cells. We characterized the structural evolution of poly(3-hexylthiophene)-*block*-poly(diketopyrrolopyrrole-terthiophene) (P3HT-*b*-DPPT-T) from solution to nanostructured thin films. Aggregation of the DPPT-T block of P3HT-*b*-DPPT-T was found in solution by small angle X-ray scattering with the P3HT block remaining well-solvated. The nanostructure in thin films was determined using a combination of wide and small angle X-ray scattering techniques as a function of processing conditions. The solution structure controlled the initial nanostructure in spin-cast thin films allowing subsequent thermal annealing processes to further improve the ordering. In contrast to the results for thin films, nanostructural ordering was not observed in the bulk samples by small angle X-ray scattering. These results suggest the importance of controlling solvent induced aggregation in forming nanostructured thin films of conjugated block co-polymers.

KEYWORDS: Semiconducting polymer, conjugated block copolymer, solution self-assembly, organic photovoltaics, thin film X-ray scattering

Introduction

The desire to build electronic devices such as organic thin film transistors (OTFTs),[1] light-emitting diodes (OLEDs),[2] photovoltaic solar cells (OPVs)[3] and thermoelectrics,[4] has propelled research in semiconducting polymers.[5–8] One of the main benefits of semiconducting polymers is their processability from organic solvents that allows thin films to be deposited using common printing methods. The electronic properties of semiconducting polymers are strongly dependent on their molecular organization in the solid state, however, making it important to develop materials such that their molecular design aids in controlling the nano- and microstructure of thin films. This factor is of particular importance for OPVs where binary blends of materials with phase separation on the nanoscale have the highest efficiency.

We report here a detailed study of the microstructure of thin films of a conjugated block copolymer (CBCPs) with semicrystalline donor and acceptor blocks. We previously reported the synthesis of poly(3-hexylthiophene)-*block*-poly(diketopyrrolopyrrole-terthiophene) (P3HT-*b*-DPPT-T) and observed nanoscale phase separated structures upon casting from solution.[9] Here, we follow the evolution of structure formation in P3HT-*b*-DPPT-T from solution to solid films to reveal the origin of the observed nanostructuring. Our results demonstrate the critical role of solution-phase aggregation in P3HT-*b*-DPPT-T and suggest pathways for structural control of block co-polymer solar cells.

The power conversion efficiency (PCE) of state-of-the-art OPVs is currently near 11 %,[10–14] but there is a significant need to increase their efficiency. The highest performing OPVs use bulk heterojunctions (BHJs), which are physical blends of an electron-donating material and an electron-accepting material.[15] In efficient BHJs, the donor and acceptor are phase separated into small (~20 nm), bicontinuous domains providing high interfacial area for charge generation and

pathways for extraction of the photogenerated charge. Post-deposition processing steps, such as thermal annealing, can either improve or reduce the PCE of BHJ OPVs by modifying the nanostructure and local order of the components. In BHJs based on polymeric donors and fullerene acceptors, the fullerene can rapidly diffuse above the glass transition of the donor polymer coarsening the phase separation and thereby lowering the PCE.[16–19] Recent work has focused on non-fullerene acceptors,[20,14] including polymers as acceptors,[21,22] which has led to high PCEs (>8%), but at this stage the morphological stability has not been studied as extensively as with fullerene-based acceptors. Thus, it would be helpful to develop morphologically stable OPVs that maintain the advantage of the nanoscale BHJ structure.

A strategy to control the nanostructure and improve the stability of OPVs is to design conjugated block copolymers (CBCPs) where one block is an electron-donating polymer and the other block is an electron-accepting polymer.[23–25] Because of the potential for controlled assembly driven by thermodynamics dictated by the molecular characteristics of the blocks, CBCP could lead to morphologically stable BHJs.[26,27] For instance, in-plane lamellar order of donor and acceptor domains would provide the interfacial area necessary for charge generation, and at the same time, the *p*- and *n*-type transport channels required for efficient collection of photogenerated charge carriers. BCPs can also be used as additives and interfacial stabilizing agents in ternary blend cells.[27,28]

The design of BCPs for single component solar cells requires that the donor and acceptor blocks not only have the appropriate length scales for phase separation, but also have the requisite electronic properties including broad optical absorption and offset transport levels for charge transport. This goal has been met by BCPs where either one block has a conjugated backbone and the other has an insulating backbone with pendant conjugated molecules,[29–37] or by

structures where both blocks have conjugated backbones (CBCPs).[38–53] Because of the relative stiffness of conjugated backbones, the phase separation of their BCP is complex due to energetic interactions between blocks, the volume fraction of the blocks, and potential crystallization. Many BCPs have a donor block based on poly(3-hexylthiophene) because of its ease of synthesis and known performance as a donor polymer in OPVs.[30,39,43,44,50,54] P3HT is a semicrystalline polymer with a relatively high melting point (>200° C), and, in many cases, the phase separation observed in its BCPs with amorphous coil blocks is driven by its crystallization limiting the ability to control structure by thermal processing.[33] In CBCPs both blocks may be semicrystalline with high melting points leading to more complex phase behavior.[23,26]

Despite complexities in understanding the phase separation of CBCPs, relatively efficient solar cells have been demonstrated with the highest reported PCEs being ~3%.[55] In these CBCP OPVs, the phase separation at ~16 nm scale of blocks of P3HT and a fluorene-benzodiathiazole-based co-polymer (PFTBT) led to solar cells with high open circuit voltage and external quantum efficiencies of ~30%. These PCEs, however, lag those of physical blends of polymers,[22,22,56–58] which have now reached ~7.7% using an acceptor based on a naphthalene diimide-selenophene copolymer acceptor and a donor based on a benzodithiophene-thieno[3,4-*b*]thiophene copolymer.[21] There are critical questions whether the differences in efficiency are simply due to materials choice, i.e. improved donor-acceptor pairs, or if the covalent linkage of the donor and acceptor in the BCP leads to detrimental recombination or interfacial electronic states.[54,59–61] Additionally, there are also significant questions concerning the role of purity of the donor and acceptor domains in BHJs on charge recombination.[62,63] A fundamental understanding of how the nanostructure and molecular order in CBCPs evolves will help to answer these questions.

We examine here how nanoscale structures form in poly(3-hexylthiophene)-*block*-poly(diketopyrrolopyrrole-terthiophene) (P3HT-*b*-DPPT-T), with the aim to elucidate how casting and thermal processing influence phase separation. We studied the solution phase structure of the polymer using small angle X-ray scattering combined with UV-Vis absorption and found clear evidence for aggregation of the DPPT-T block. The resulting short range order and longer range order in the solid state was examined using complementary hard and soft X-ray scattering methods as a function of thermal annealing. In contrast to other CBCPs, aggregation and crystallization of DPPT-T rather then P3HT drove structure formation. The initial structure in thin films driven by this solution-phase structure can be further modified through thermal annealing.

Results and Discussion

Molecular Design of P3HT-b-DPPT-T As previously described, poly(3-hexylthiophene)-*block*-poly(diketopyrrolopyrrole-terthiophene) (P3HT-*b*-DPPT-T) (**Figure 1**) was synthesized using a strategy involving the Stille coupling of end-functional P3HT and two sets of end-functionalized monomer units that comprise the DPPT-T block.[9] The number-averaged molecular weight (M_n) and polydispersity index (PDI) of the block copolymer were 37.2 kDa and 1.86, respectively, with a molar repeat ratio of 87/13 for P3HT/DPPT-T. DPPT-T has a low optical gap relative to P3HT, with primary absorbances in the range of 700 – 800 nm and 500 – 600 nm, respectively. The optical absorption of the block co-polymers reflects the complementary absorption profiles of the two blocks and provides broad coverage of the solar spectrum (**Figure 1)**.

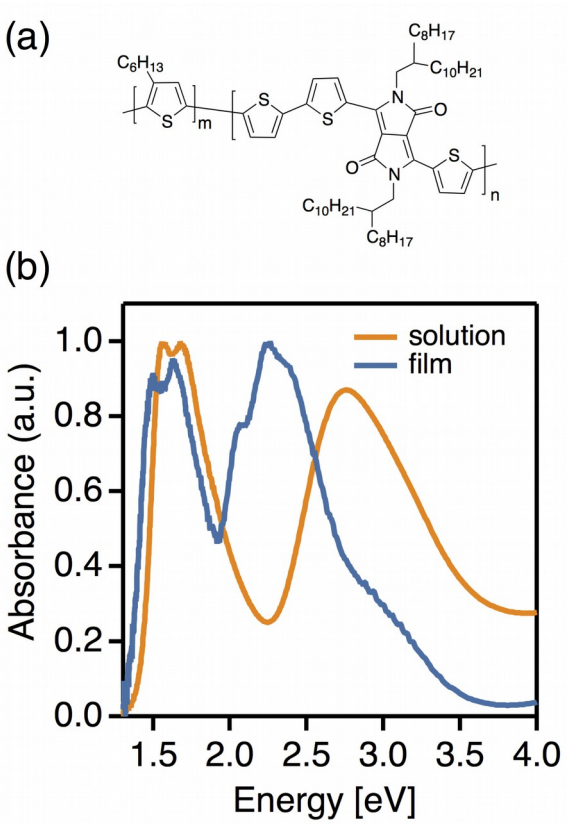

Figure 1. (a) Molecular structure and **(b)** UV-VIS. absorption spectra of P3HT-*b*-DPPT-T in ortho-dichlorobenzene solution and in a thin film.

P3HT-b-DPPT-T Aggregates in Solution. The optical absorption of the P3HT and DPPT-T blocks shows substantially different behavior upon solidification from the solvent, *ortho*-dichlorobenzene (*o*-DCB). The red-shift of the peak at 2.75 eV upon solidification to 2.26 eV suggests that P3HT is well-solvated in solution and undergoes a significant structural organization upon film casting, while the low energy peaks centered at 1.63 eV from DPPT-T show little change. The lack of a red-shift and the vibronic structure suggests aggregation of the DPP-T block in solution. Temperature-dependent UV-Vis spectra of P3HT-*b*-DPPT-T and DPPT-T solutions show relatively small changes up to 140°C, near the solvent's boiling point (**Figure**

S1). The aggregation of DPPT-T in *o*-DCB is common for DPP-based polymers[64,65] and the spectra suggest that aggregation is not substantially changed in the block copolymer.

The UV-Vis spectra suggest aggregation of the DPPT-T block, but also indicate that the P3HT block remains well-solvated. To verify that aggregation was the origin of the lack of a shift in the optical absorption rather than the stiffness of the DPPT-T block, solution-phase small angle X-ray scattering (SAXS) was performed in *o*-DCB at a concentration equivalent to that used in thin film coating (15 mg/mL). 2D SAXS scattering patterns were acquired by transmission of a 14 keV beam through a temperature-controlled liquid flow cell and azimuthally integrated to obtain line profiles (**Figure 2**).[48] As the temperature is decreased towards room temperature from 80 °C where the block copolymer is dissolved, aggregation becomes increasingly pronounced. A weak scattering peak, centered at a scattering vector of 3.0 nm^{-1}, which is similar to *(100)*

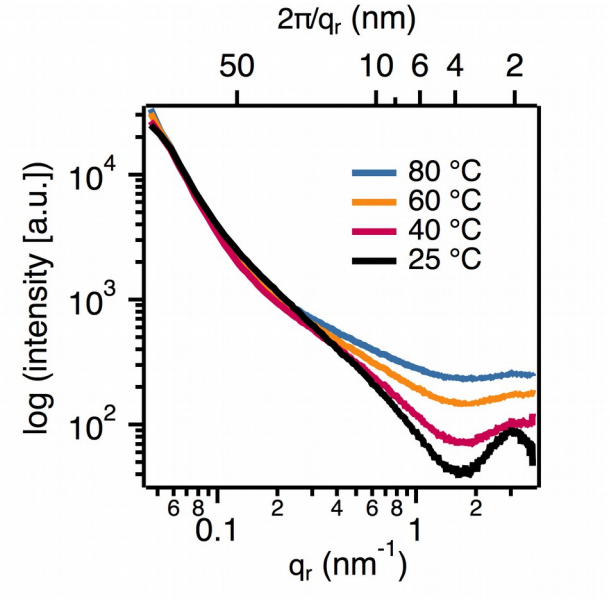

Figure 2. Temperature-dependent solution transmission SAXS of P3HT-*b*-DPPT-T in *o*-DCB at a concentration of 15 mg/mL. Line profiles were generated from the radial integration of scattering images

spacing of crystalline DPPT-T or P3HT in the solid,[66] is increasingly observed as the solution

temperature is decreased. At $\boldsymbol{q}$ below 0.1 nm^{-1}, the scattering intensity falls off as $\boldsymbol{q}^{-2.7}$ for all temperatures without evidence of a Gunier region, i.e. a plateau, within the limits of the experimental range. Another region is observed until $\mathbf{q} \sim 1$ nm^{-1}, where the scattering intensity scales as $\boldsymbol{q}^{-1.3}$ at high temperature and as $\boldsymbol{q}^{-1.5}$ at room temperature. These values are between what is expected for rods (q^{-1}) and sheets or discs (q^{-2}). Overall, we interpret these results as evidence for aggregation of the polymer chains with rod-like regions within them. These data along with the UV-Vis spectra as a function of temperature suggest that the DPPT-T block is the origin of the aggregation; while we cannot perfectly rule out some aggregation of the P3HT block, spectroscopy suggests that it is well solvated relative to DPPT-T.

We can further compare the scattering from homopolymers to the P3HT-*b*-DPPT-T block polymer to examine whether the aggregation is driven by the block structure. Solution SAXS of P3HT is known to show coil-like behavior in *o*-DCB[67] and we examined DPPT-T homopolymers here (**Figure S2**). A similar length scale of alkyl-stacking structure (centered at ~3.0 nm^{-1}) is observed for the DPPT-T homopolymer as for P3HT-*b*-DPPT-T at temperatures to 60°C. The scattering follows a $\boldsymbol{q}^{-1.1}$ form between 0.1 and 1 nm^{-1} suggesting a rod-like structure and scaling as q^{-3} at low **q** indicating larger scale aggregation. Solution SAXS of co-polymers of furan and DPP show similar features indicating aggregation, i.e. a peak emerging near the layering expected in the solid state, suggesting such behavior may be common for DPP-based, and perhaps other, polymers.[68] Based on the UV-Vis spectra and solution-phase SAXS, we therefore believe that the DPPT-T block begins to form structured aggregates in solution, while the P3HT segments are in a more coil-like configuration. This aggregation in solution likely has a substantial role in the formation of the nanoscale phase separated structures previously observed in thin films. While we expect that reducing the concentration will decrease the aggregation, but

we did not explore such conditions because the concentration used here is required to form ~100 nm thick films relevant for solar cells.

Ordering of P3HT-b-DPPT-T in Bulk. In order to understand how thermal processing drives nanostructure formation in P3HT-*b*-DPPT-T, we examined both short and longer range order using X-ray scattering as a function of temperature. Differential scanning calorimetry (DSC) of P3HT-*b*-DPPT-T powder shows well-defined melting and crystallization transitions for both the P3HT and DPPT-T blocks (**Figure S4**). Specifically the P3HT block melts at ~220 °C ($T_{m,\ P3HT}$) and recrystallizes at ~180 °C ($T_{c,\ P3HT}$) upon cooling in agreement with literature values for the homopolymer,[69,70] while the DPPT-T block melts at ~260 °C ($T_{m,\ DPPT\text{-}T}$) and recrystallizes at ~245 °C ($T_{c,\ DPPT\text{-}T}$). The well-separated thermal transitions for each block provides a thermal window in which to investigate the structural effects of isothermal annealing and controlled cooling.

To further understand crystallization of P3HT-*b*-DPPT-T in bulk and to verify the assignment of thermal transitions from DSC, transmission WAXS was collected during heating under the same conditions as for the conventional DSC measurement. Shown in **Figure 3** are radially averaged WAXS line profiles, for temperatures below and above the melting transition of each block, in the *(100)* alkyl-stacking region. It is seen from the trace at room temperature that, as expected, the *(100)* peak from P3HT is present near 3.7 nm^{-1}, and the *(100)* peak from DPPT-T is at 2.9 nm^{-1}. In physical blends of poly(alkyl-thiophene) and co-polymers of DPP and thiophene,

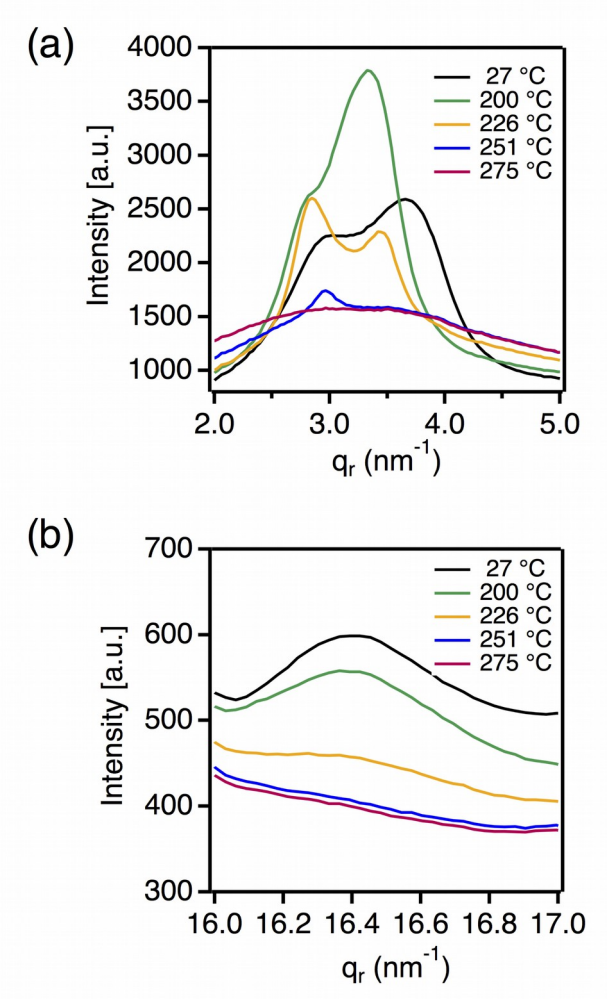

Figure 3. Temperature dependent-WAXS for bulk powder of P3HT-*b*-DPPT-T near the **(a)** (100) position for the alkyl-stacking region and the **(b)** (010) π-stacking region (the scattering curves are vertically offset for clarity).

alloying behavior has been observed in thin films with a single *d*-spacing present[71] and some

block co-polymers of poly(alkylthiophenes) show co-crystallization. In contrast, the block co-polymers here show distinct crystalline phases for each block allowing us to readily identify the thermal transitions from DSC. As the temperature is elevated, both peaks shift to lower scattering vectors due to thermal expansion. The higher ***q*** P3HT peak begins to decay in intensity near the P3HT melting transition and is completely absent at 250 °C. At this temperature, the lower ***q*** DPPT-T peak is still present but also disappears once the DPPT-T melting transition is crossed. Similarly, **Figure 2(c)** depicts radially averaged, temperature-dependent DSC-WAXS traces for the *(010)* π-stacking region. Here, a broad π-stacking peak is centered near 16.4 nm^{-1} near the expected *d*-spacings for P3HT and DPPT-T homopolymers. The π-stacking feature broadens at temperatures below the DPPT-T melt, but the alkyl layering of DPPT-T is still present. This observation suggests that either the π-stacking is mostly due to the P3HT block or that the melting of P3HT disrupts the π-stacking in the DPPT-T block due to their covalent linkage.

Transmission SAXS studies were also conducted on the P3HT-*b*-DPPT-T powder to investigate how the crystalline thermal transitions are related to domain formation in the bulk material. Between room temperature and 275 °C no obvious features were evident over the length scales of 5 – 100 nm (**Figure S5**). Instead, an exponentially decaying profile was observed, suggesting that, within this length scale range, there is no unique length scale of separation between the two blocks or that their electron density is too close to provide scattering contrast. These results contrast observations for block co-polymers of P3HT and polyfluorenes where phase separation could be observed in bulk SAXS.[39,46] In those cases the backbone structures have very different molecular architecture due to the alkylation of the bridge-head position in the fluorene group relative to the planar DPP and thiophene units in P3HT and DPPT-

T. Therefore, the DSC-SAXS data does not reveal phase separated structures in the bulk on the time scales examined; these results contrast our previous results demonstrating nanostructured domains in solution-cast thin films of P3HT-*b*-DPPT-T.[9]

Crystalline and Nanostructure of Solution-Cast Films. The majority of organic thin film electronic devices are made by solution-casting and here we can use our understanding of the structure in solution to interpret the structure formation upon spin-casting. Previously, we reported initial data on the structure of films cast from solvent followed by annealing with rapid quenching.[9] Here we modify the thermal annealing process to investigate and tune the structure formation leading to better structural order than previously observed.

Both blocks in P3HT-*b*-DPPT-T films show crystalline ordering that can be modified by annealing the thin films near the melt transitions for the blocks. 2-D GIWAXS patterns are presented in **Figure 4**, for the as cast film and following annealing at 200 °C, 225 °C, and 265 °C for 1 hour and slow-cooling back to room temperature (rate of 4 °C/min). In our previously

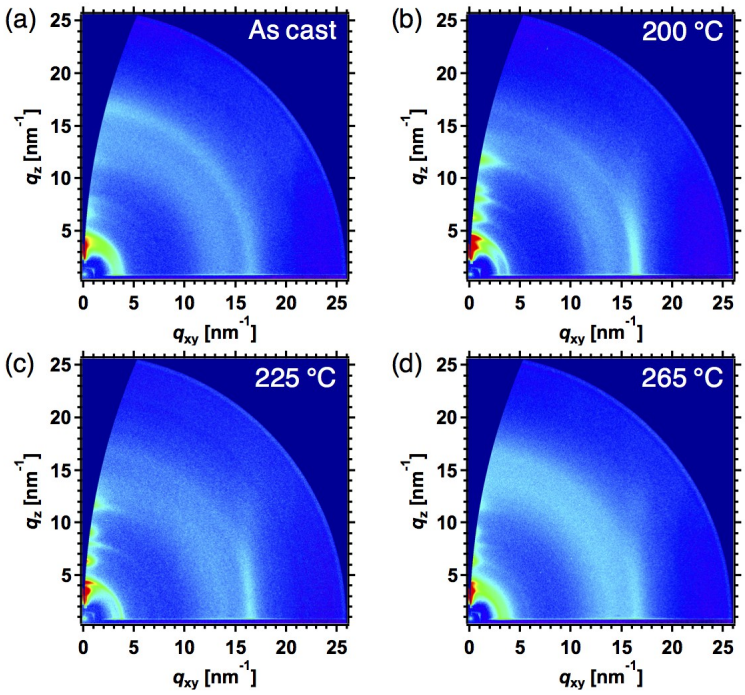

Figure 4 2-D GIWAXS patterns of P3HT-*b*-DPPT-T thin films: **(a)** as cast and after isothermal annealing for 1 h at **(b)** 200 °C, **(c)** 225 °C, and **(d)** 265 °C.

reported work, films that were annealed and quenched quickly to room temperature show qualitatively similar scattering features.[9] It is apparent from GIWAXS that the local structure of both P3HT and DPPT-T blocks in thin films is similar to their bulk structure, with $(100)_{P3HT}$ and $(100)_{DPPT\text{-}T}$ peaks appearing at q=3.7 and 2.9 nm^{-1}, respectively, in the as-cast film with only slight shifts relative to the respective homopolymers.[66,72] Relatively broad peaks are observed for the P3HT and DPPT-T blocks in the as-cast film, prior to any annealing. Following thermal annealing at 200°C, the peaks in the nearly out-of-plane direction become more well-defined and narrow (**Figure 5**). The thermal annealing process also enhances the ordering of both crystalline structures, with the presence of *(200)*, *(300)*, and *(400)* DPPT-T peaks, and *(200)* and *(300)* P3HT peaks for all thermally annealed films. For films annealed at 225° C and 265 °C, where the melt states of P3HT and DPPT-T are accessed, respectively, the alkyl-stacking crystalline structure of each block is able to recover due to the slow rate of cooling through each crystallization transition. Once DPPT-T is melted, the peak width in GIWAXS are slightly broadened (~10%). Similar behavior is observed in-plane from the π-stacking of the chains **Figure 5b**. The major peak at 16.4 nm^{-1} originates from the co-facial stacking of the backbones and cannot be readily assigned to P3HT or DPPT-T domains due to the similarity of the spacing for the two materials.[66,72] In the as-cast film, this peak is broadest (FWHM = 0.26 $Å^{-1}$), suggesting very disordered π-stacking, but narrows substantially following annealing and cooling from 200 °C (cold crystallization conditions, FWHM = 0.13 $Å^{-1}$) and 225 °C (P3HT melt annealing conditions, FWHM= 0.16 $Å^{-1}$. When the film is annealed and cooled from the DPPT-T melt, the peak broadens (FWHM= 0.21 $Å^{-1}$) to a width closer to the as-cast state.

Both crystallites of P3HT and DPPT-T are oriented in an edge-on fashion, in which the alkyl-

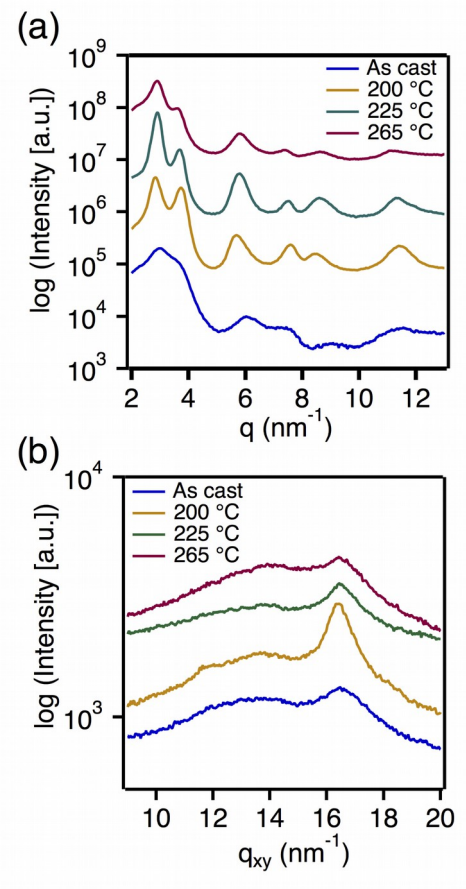

Figure 5 (a) GIWAXS intensity along the missing wedge close to q_z and **(b)** the in-plane direction q_{xy} of P3HT-*b*-DPPT-T thin films: **(a)** as-cast and after isothermal annealing for 1 h at **(b)** 200 °C, **(c)** 225 °C, and **(d)** 265 °C.

stacking is dominant in the out-of-plane direction, while the π-stacking vector is primarily in the in-plane direction (**Figure 3(a-d)**). These observations show that DPPT-T and P3HT forms disordered crystallites upon casting and they both improve their structural order upon annealing even below the melt temperatures of the blocks. The difference in the d(100)-spacing of the two blocks (4 Å) suggests there is likely a region of disorder at their junction. The P3HT block has a higher MW than DPPT-T which likely allows it to accommodate the change in layer spacing between the two blocks. The suppressed crystallization temperature of the P3HT block in P3HT-

b-DPPT-T relative to the same transition for P3HT homopolymer (see **Figure S4**) further suggests that ordering of the DPPT-T block impacts the the undercooling required to recrystallize the P3HT block.

GIWAXS data reveals that the crystalline domains within P3HT-*b*-DPPT-T are textured in an edge-on geometry (the *a**-axis aligned closely with the surface normal), but does not reveal the longer range structure. The blocks in P3HT-*b*-DPPT-T studied here have relatively low molecular weight and are quite short, with the P3HT block being approximately 48 repeat units long and the DPPT-T block approximately 7 repeat units long. Overall, we estimate that the length of an extended chain is ~30 nm. The P3HT block is below the molecular weight for chain bending,

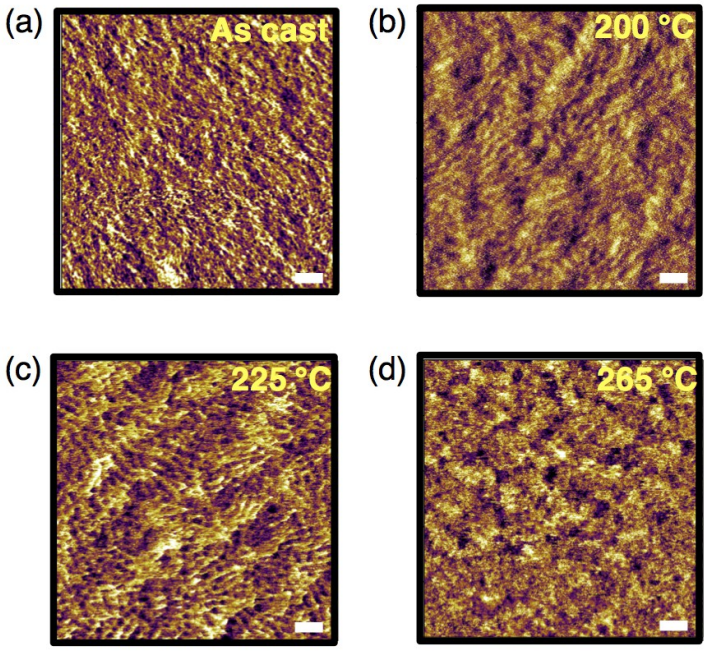

Figure 6. Atomic force microscopy phase-contrast images of P3HT-*b*-DPPT-T thin films for four different conditions: **(a)** as cast and isothermally annealed at **(b)** 200 °C, **(c)** 225 °C, and **(d)** 265 °C. Following all isothermal annealing conditions, films were slowly cooled to below the P3HT crystallization transition at 4 °C/min. In each image, the scale bar represents 100 nm.

estimated to be approximately 12 kDa,[73] and the DPPT-T block is relative short. We therefore

expect that the polymer chains are in their extended conformation in thin films. Because of the texture of the ordered domains, a lamellar morphology is likely.

Atomic force microscopy (AFM) of the slow cooled films reveals nanostructuring at the block copolymer thin film-air interface (**Figure 6 and Figure S6-S8**). In the as-cast film, the surface has a disordered topography suggesting by the weak separation of donor and acceptor blocks. However, for the film annealed at 200 °C under cold crystallization conditions for P3HT and DPPT-T and slowly cooled, a lamellar structure becomes apparent and further evolves when the annealing temperature is increased to 225 °C. These features are approximately 50 nm in width and persist over length scales greater than 100 nm. This domain spacing is close to twice the contour length of the block copolymer chain. When the film is annealed at 265 °C and slowly cooled, the surface morphology returns to a disordered domain structure, although coarsened relative to the as-cast condition. This change is correlated to the higher disorder in the crystallites observed in GIWAXS suggesting that maintaining crystallinity of one block is critical in developing the fiber-like domains that are observed using intermediate annealing conditions.

Because AFM only measures the surface morphology of block copolymer thin films,

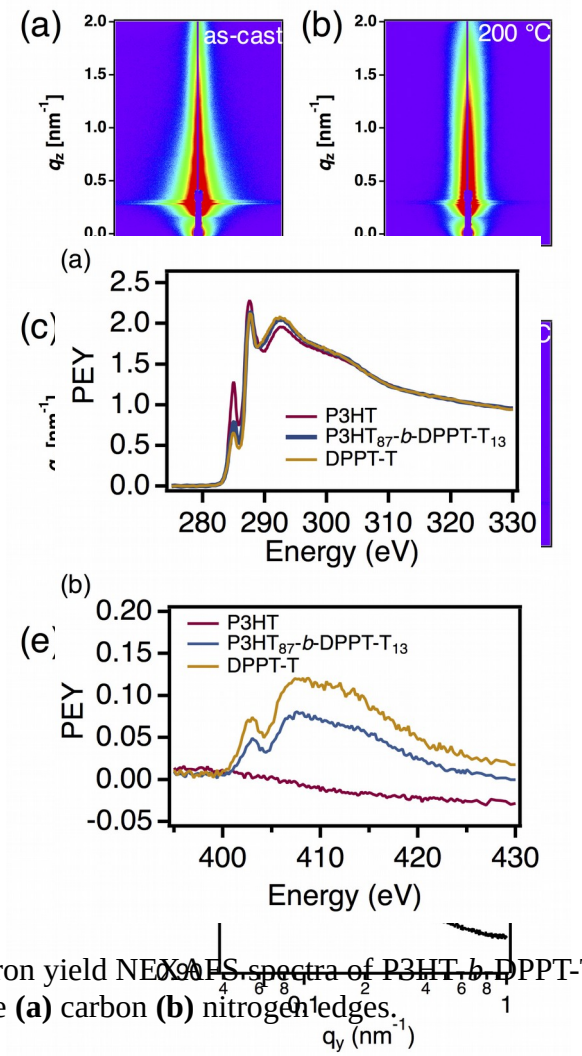

Figure 8. Partial electron yield NEXAFS spectra of P3HT-*b*-DPPT-T and P3HT and DPPT-T homopolymers at the **(a)** carbon **(b)** nitrogen edges.

Figure 7. GISAXS data set of P3HT-*b*-DPPT-T thin films for four different conditions: **(a)** as cast and isothermally annealed at **(b)** 200 °C, **(c)** 225 °C, and **(d)** 265 °C. Following all isothermal annealing conditions, films were slowly cooled to below the P3HT crystallization transition at 4 °C/min. **(e)** GISAXS in-plane line integrations along the Yoneda peak for all four processing conditions (curves are shifted in intensity for clarity).

additional analysis is needed to confirm that this structure persists throughout the thickness of the film. Hard X-ray GISAXS shows that annealing at 225 °C, where AFM shows clearly defined domains, leads to a well-defined peak centered at a value that corresponds to a center-to-center domain spacing of 52 nm (**Figure 7**). The GISAXS pattern from the film annealed at 200 °C

indicates that the low-q_y broadens, relative to the as-cast state, and that this ultimately leads to the more well-defined structure at 225 °C. Moreover, the choice of incident angle in this GISAXS experiment (0.18°) probes the bulk of the film depth, confirming that this domain structure persists throughout the film and does not only exist at the film-air interface. Finally, to highlight the importance of slow cooling in generating these ordered domain structures, GISAXS was performed on films annealed under the same conditions but that were quenched from elevated temperature (**Figure S9**). Quenching does not provide a sufficient time scale for recrystallization of the DPPT-T along the fiber-like axis, and thus no ordered domain structures are observed.

To complement the GISAXS and AFM data, we also carried out resonant soft X-ray scattering (RSoXS) using a transmission geometry that probes the bulk of the films. The use of resonant contrast from absorption of soft X-rays increases the interaction length with the sample and can provide information from differences in chemical structure as well.[74–76] Near edge X-ray absorption fine structure (NEXAFS) spectra of as-cast films of P3HT and DPPT-T homopolymers and their block co-polymer showed clear spectral differences near the carbon and nitrogen edges (Figure 8). While the spectral signatures for each polymer are similar at the carbon edge, the do provide scattering contrast near the π* resonances from the conjugated backbones and carbonyl group in the DPP block (**Figure S9**).[46] Moreover, because only the DPPT-T polymer has a nitrogen atom in the monomer, there is additionally spectroscopic contrast near the nitrogen edge.[45]

Resonant soft X-ray scattering (RSoXS) was conducted, in a transmission geometry through

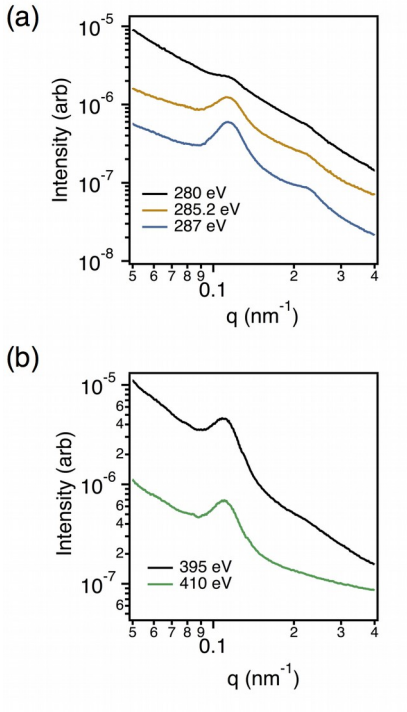

Figure 9. Transmission RSoXS of a P3HT-*b*-DPPT-T thin film annealed at 225 °C and slowly cooled near **(a)** the carbon and **(b)** the nitrogen edge. The scattering intensity was radially integrated and the data is offset for clarity.

the P3HT-*b*-DPPT-T thin film, for the sample annealed at 225 °C and slowly cooled. **Figure 9** presents the radially integrated RSoXS profile for several incident energies, collected near the carbon and nitrogen edges further confirming the high level of domain ordering observed with AFM and GISAXS. The primary $\boldsymbol{q}^*$ and secondary $2\boldsymbol{q}^*$ peaks are clearly observed at 285.2 eV and 287 eV (at $\boldsymbol{q}^* = 0.14$ nm^{-1}) and are representative of a center-to-center lamellar domain spacing of 55 nm (**Figure 9a**) in good agreement with the GISAXS data. We note that the enhanced contrast from RSoXS allowed the observation of the higher order peak which was absent in the GISAXS data. A similar length scale of 57 nm is seen in the nitrogen edge data (**Figure 9b**). RSoXS suggests a lamellar arrangement of alternating P3HT donor and DPPT-T acceptor regions, consistent with the domain structure observed by AFM and the dominant

orientation of the crystalline chains is edge-on from the GIWAXS (**Figure 4**). Due to the similar size of each domain, its not possible to ascribe the regions of the phase-contrast AFM images in **Figure 6** using RSoXS. In addition, the transmission scattering geometry and averaged through-depth film structure from RSoXS again supports the connection between the bulk and surface structure. These data indicate that alternating regions of donor and acceptor are present in these films at length scales relevant for OPVs. It is worth noting that although it would be ideal to determine a chi-parameter, it is difficult for materials that crystallize like both of these polymer blocks. In addition, a difficulty with materials with sidechain structures as these is that surface energy will likely reflect the alkylated chains, but not reveal much detail about the interaction between the conjugated backbones, which are likely to have a strong influence on miscibility.

Structure Formation from Solution to Films. Our physical characterization of the solution and solid state suggest the pathway for forming nanoscale phase separated structures in thin films. A schematic that displays the ordering and primary orientation of P3HT and DPPT-T crystallites and the larger scale lamellar arrangement of alternating donor and acceptor fiber-like domains is shown **Figure 10**. Due to solvent quality mismatch between the two blocks, DPPT-T aggregates in solution, and upon film casting, this structure is retained and enhanced during thermal annealing. By melting and recrystallizing the P3HT domains, fiber-like domains of donor and

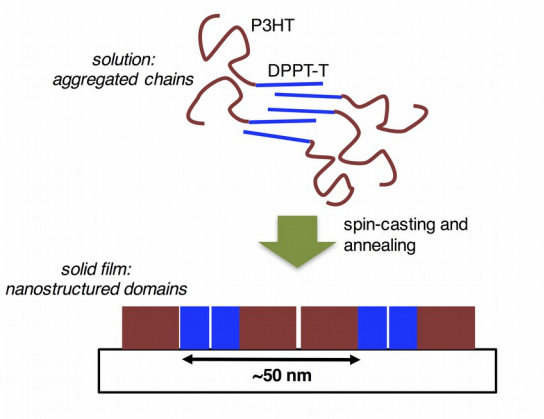

Figure 10. Schematic showing aggregation of P3HT-*b*-DPPT-T in solution and the subsequent structure in thin films.

acceptor are formed. GISAXS, RSoXS, and AFM show a domain spacing of fibrils that can be attributed to a lamellar arrangement of extended chains. The estimated contour length of a chain is ~30 nm while the spacing from RSoXS is 55 nm; we expect that the contour length is overestimated due to a typical overestimation of polystyrene-equivalent MW by GPC.[77] This observation suggests that *two* block copolymer chains extend across the fibril width with first and second order scattering peaks suggesting significant structural order. Our bulk SAXS data does not show clear structure formation between the blocks under similar conditions suggesting that aggregation in solution is critical to forming the observed nanostructures in thin films. In contrast to many block co-polymers where crystallization of P3HT can help to drive the structure formation,[33,37,39] here DPPT-T drives the structure formation because it aggregates first. In the polymer studied here, the P3HT block has a larger weight fraction (~20% higher) in the polymer, yet the DPPT-T block is dominant. This result contrasts that observed in CBCPs of P3HT with polyfluorenes where the weight fraction of the polymer was found to control which block dominates the initial ordering.[39,78] The melt temperature of DPPT-T is higher than that for P3HT, but the difference is not large indicating that aggregation (solvent quality) has a more critical role than molecular weight for this system.

Conclusion.

In conclusion, we have investigated the structural evolution of the conjugated block copolymer P3HT-*b*-DPPT-T from the solution state to the solid state. The nanoscale morphology is hierarchical in nature, comprising textured and ordered crystallites of donor and acceptor blocks, and on a larger scale, a lamellar arrangement of alternating donor and acceptor fibrillar domains. The assembly of these structures is driven by aggregation in solution and subsequent

crystallization of primarily the DPPT-T block, and is less influenced by microphase separation under these casting conditions. These results suggest that solvents can be used to drive the nanoscale structure in thin films of conjugated block copolymers and tuned by thermal annealing. The resulting nanostructures have appropriate length scales for BHJ solar cells and can enable the study of exciton migration and dissociation and charge extraction. The understanding developed here for structure formation in conjugated block copolymers will be very useful in order to engineer highly ordered and thermally controllable bulk heterojunction organic photovoltaics.

ASSOCIATED CONTENT

SUPPORTING INFORMATION

Temperature-dependent solution-state UV-*vis.* absorption spectroscopy; Differential scanning calorimetry data; phase-, height-, and amplitude-contrast AFM micrographs; additional solution and bulk SAXS and GISAXS data. This material is available free of charge via the Internet at http://pubs.acs.org.

AUTHOR INFORMATION

Corresponding Author
*(MLC) E-mail: mchabinyc@engineering.ucsb.edu

⋂ EJK deceased December 2014

Present Addresses

M.A.B.: Lawrence Berkeley National Laboratory, Berkeley, CA

S.-Y.K.: The Dow Chemical Company, Freeport, TX

L.A.P.: Apeel Sciences, Santa Barbara, CA

Author Contributions

MAB and SYK contributed equally to the manuscript. This manuscript was prepared through contributions of all authors. All authors have given approval to the final version of the manuscript.

Notes
The authors declare no competing financial interests.

ACKNOWLEDGMENTS

MAB acknowledges support from National Science Foundation and California NanoSystems Institute Graduate Research Fellowships and an Advanced Light Source Doctoral Fellowship. MLC and HA were supported by NSF DMR 1207549 and 1207032. The authors would like to thank the SAXS/WAXS team at Beamline 7.3.3, including Dr. Eric Schaible, Dr. Ilja Günkel, and Dr. Chenhui Zhu, and the Soft X-ray Scattering team at Beamline 11.0.1.2, including Dr. Anthony Young, of the Advanced Light Source at Lawrence Berkeley National Lab for their help with the GIWAXS, GISAXS, RSoXS, and NEXAFS measurements; Dr. Cherno Jaye and Dr. Dan Fischer of Beamline U7A at the National Synchrotron Light Source at Brookhaven National Laboratory for their assistance with NEXAFS experiments; Dr. Charles Troxel, Jr. and Dr. Badri Shyam of Beamline 2-1, Ron Marks of Beamline 7-2, Dr. Chris Tassone, Dr. Alex Ayzner, Dr. Chad Miller, and Dr. Stefan Mannsfeld of Beamline 11-3 at the Stanford Synchrotron Radiation Lightsource at SLAC National Accelerator Laboratory for their assistance with GIWAXS and XRD measurements. This work made use of the UCSB Materials Research Laboratory Central Facilities, supported by the MRSEC Program of the National Science Foundation under award No. DMR 1121053. Use of the Advanced Light Source, Lawrence Berkeley National Laboratory, was supported by the Director, Office of Science, Office of Basic Energy Sciences, of the U.S. Department of Energy, under Contract No. DE-AC02-05CH11231. Use of the Stanford Synchrotron Radiation Lightsource, SLAC National Accelerator Laboratory, was supported by the U.S. Department of Energy, Office of Science, Office of Basic Energy Sciences, under Contract No. DE-AC02-76SF00515. Use of the National Synchrotron Light Source, Brookhaven National Laboratory, was supported by the U.S. Department of Energy, Office of Science, Office of Basic Energy Sciences, under Contract No. DE-AC02-98CH10886. Prof. Karen Winey is gratefully thanked for valuable discussions.

REFERENCES

(1) Sirringhaus, H. 25th Anniversary Article: Organic Field-Effect Transistors: The Path Beyond Amorphous Silicon. *Adv. Mater.* **2014**, *26* (9), 1319–1335.

(2) Reineke, S.; Thomschke, M.; Lüssem, B.; Leo, K. White Organic Light-Emitting Diodes: Status and Perspective. *Rev. Mod. Phys.* **2013**, *85* (3), 1245–1293.

(3) Dou, L.; You, J.; Hong, Z.; Xu, Z.; Li, G.; Street, R. A.; Yang, Y. 25th Anniversary Article: A Decade of Organic/Polymeric Photovoltaic Research. *Adv. Mater.* **2013**, *25* (46), 6642–6671.

(4) Zhang, Q.; Sun, Y.; Xu, W.; Zhu, D. Organic Thermoelectric Materials: Emerging Green Energy Materials Converting Heat to Electricity Directly and Efficiently. *Adv. Mater.* **2014**, *26*, 6829-6851.

(5) Zhou, H.; Yang, L.; You, W. Rational Design of High Performance Conjugated Polymers for Organic Solar Cells. *Macromolecules* **2012**, *45* (2), 607–632.

(6) Son, H. J.; Carsten, B.; Jung, I. H.; Yu, L. Overcoming Efficiency Challenges in Organic Solar Cells: Rational Development of Conjugated Polymers. *Energy Environ. Sci.* **2012**, *5* (8), 8158.

(7) Son, H. J.; He, F.; Carsten, B.; Yu, L. Are We There yet? Design of Better Conjugated Polymers for Polymer Solar Cells. *J. Mater. Chem.* **2011**, *21* (47), 18934.

(8) Holliday, S.; Donaghey, J. E.; McCulloch, I. Advances in Charge Carrier Mobilities of Semiconducting Polymers Used in Organic Transistors. *Chem. Mater.* **2014**, *26* (1), 647–663.

(9) Ku, S.-Y.; Brady, M. A.; Treat, N. D.; Cochran, J. E.; Robb, M. J.; Kramer, E. J.; Chabinyc, M. L.; Hawker, C. J. A Modular Strategy for Fully Conjugated Donor-Acceptor Block Copolymers. *J. Am. Chem. Soc.* **2012**, *134* (38), 16040–16046.

(10) Yang, T.; Wang, M.; Duan, C.; Hu, X.; Huang, L.; Peng, J.; Huang, F.; Gong, X. Inverted Polymer Solar Cells with 8.4% Efficiency by Conjugated Polyelectrolyte. *Energy Environ. Sci.* **2012**, *5* (8), 8208.

(11) He, Z.; Xiao, B.; Liu, F.; Wu, H.; Yang, Y.; Xiao, S.; Wang, C.; Russell, T. P.; Cao, Y. Single-Junction Polymer Solar Cells with High Efficiency and Photovoltage. *Nat. Photonics* **2015**, *9* (3), 174–179.

(12) Small, C. E.; Chen, S.; Subbiah, J.; Amb, C. M.; Tsang, S.-W.; Lai, T.; Reynolds, J. R.; So, F. High-Efficiency Inverted Dithienogermole-Thienopyrrolodione-Based Polymer Solar Cells. *Nat. Photonics* **2012**, *6* (2), 115–120.

(13) Liu, Y.; Zhao, J.; Li, Z.; Mu, C.; Ma, W.; Hu, H.; Jiang, K.; Lin, H.; Ade, H.; Yan, H. Aggregation and Morphology Control Enables Multiple Cases of High-Efficiency Polymer Solar Cells. *Nat. Commun.* **2014**, *5*, 5293.

(14) Zhao, W.; Qian, D.; Zhang, S.; Li, S.; Inganäs, O.; Gao, F.; Hou, J. Fullerene-Free Polymer Solar Cells with over 11% Efficiency and Excellent Thermal Stability. *Adv. Mater.* **2016**.

(15) Janssen, R. A. J.; Nelson, J. Factors Limiting Device Efficiency in Organic Photovoltaics. *Adv. Mater.* **2013**, *25* (13), 1847–1858.

(16) Treat, N. D.; Chabinyc, M. L. Phase Separation in Bulk Heterojunctions of Semiconducting Polymers and Fullerenes for Photovoltaics. *Annu. Rev. Phys. Chem.* **2014**, *65* (1), 59–81.

(17) Treat, N. D.; Shuttle, C. G.; Toney, M. F.; Hawker, C. J.; Chabinyc, M. L. In Situ Measurement of Power Conversion Efficiency and Molecular Ordering during Thermal Annealing in P3HT:PCBM Bulk Heterojunction Solar Cells. *J. Mater. Chem.* **2011**, *21* (39), 15224–15231.
(18) Wong, H. C.; Li, Z.; Tan, C. H.; Zhong, H.; Huang, Z.; Bronstein, H.; McCulloch, I.; Cabral, J. T.; Durrant, J. R. Morphological Stability and Performance of Polymer–Fullerene Solar Cells under Thermal Stress: The Impact of Photoinduced PC60BM Oligomerization. *ACS Nano* **2014**.
(19) Schroeder, B. C.; Li, Z.; Brady, M. A.; Faria, G. C.; Ashraf, R. S.; Takacs, C. J.; Cowart, J. S.; Duong, D. T.; Chiu, K. H.; Tan, C.-H.; Cabral, J. T.; Salleo, A.; Chabinyc, M. L.; Durrant, J. R.; McCulloch, I. Enhancing Fullerene-Based Solar Cell Lifetimes by Addition of a Fullerene Dumbbell. *Angew. Chem. Int. Ed.* **2014**, *53* (47), 12870–12875.
(20) Nielsen, C. B.; Holliday, S.; Chen, H.-Y.; Cryer, S. J.; McCulloch, I. Non-Fullerene Electron Acceptors for Use in Organic Solar Cells. *Acc. Chem. Res.* **2015**, *48* (11), 2803–2812.
(21) Hwang, Y.-J.; Courtright, B. A. E.; Ferreira, A. S.; Tolbert, S. H.; Jenekhe, S. A. 7.7% Efficient All-Polymer Solar Cells. *Adv. Mater.* **2015**, *27* (31), 4578–4584.
(22) Zhou, Y.; Kurosawa, T.; Ma, W.; Guo, Y.; Fang, L.; Vandewal, K.; Diao, Y.; Wang, C.; Yan, Q.; Reinspach, J.; Mei, J.; Appleton, A. L.; Koleilat, G. I.; Gao, Y.; Mannsfeld, S. C. B.; Salleo, A.; Ade, H.; Zhao, D.; Bao, Z. High Performance All-Polymer Solar Cell via Polymer Side-Chain Engineering. *Adv. Mater.* **2014**, *26* (22), 3767–3772.
(23) Lee, Y.; Gomez, E. D. Challenges and Opportunities in the Development of Conjugated Block Copolymers for Photovoltaics. *Macromolecules* **2015**, *48* (20), 7385–7395.
(24) Sommer, M.; Huettner, S.; Thelakkat, M. Donor–acceptor Block Copolymers for Photovoltaic Applications. *J. Mater. Chem.* **2010**, *20* (48), 10788.
(25) Darling, S. B. Block Copolymers for Photovoltaics. *Energy Environ. Sci.* **2009**, *2* (12), 1266.
(26) Kipp, D.; Verduzco, R.; Ganesan, V. Design of Bicontinuous Donor/acceptor Morphologies for Use as Organic Solar Cell Active Layers. *J. Polym. Sci. Part B Polym. Phys.* **2016**, *54* (9), 884–895.
(27) Kipp, D.; Mok, J.; Strzalka, J.; Darling, S. B.; Ganesan, V.; Verduzco, R. Rational Design of Thermally Stable, Bicontinuous Donor/Acceptor Morphologies with Conjugated Block Copolymer Additives. *ACS Macro Lett.* **2015**, *4* (9), 867–871.
(28) Mulherin, R. C.; Jung, S.; Huettner, S.; Johnson, K.; Kohn, P.; Sommer, M.; Allard, S.; Scherf, U.; Greenham, N. C. Ternary Photovoltaic Blends Incorporating an All-Conjugated Donor–Acceptor Diblock Copolymer. *Nano Lett.* **2011**, *11* (11), 4846–4851.
(29) Koyuncu, S.; Wang, H.-W.; Liu, F.; Toga, K. B.; Gu, W.; Russell, T. P. A Novel Complementary Absorbing Donor–acceptor Pair in Block Copolymers Based on Single Material Organic Photovoltaics. *J. Mater. Chem. A* **2014**, *2* (9), 2993.
(30) Gupta, G.; Singh, C. R.; Lohwasser, R. H.; Himmerlich, M.; Krischok, S.; Müller-Buschbaum, P.; Thelakkat, M.; Hoppe, H.; Thurn-Albrecht, T. Morphology, Crystal Structure and Charge Transport in Donor–Acceptor Block Copolymer Thin Films. *ACS Appl. Mater. Interfaces* **2015**, *7* (23), 12309–12318.
(31) Lindner, S. M.; Hüttner, S.; Chiche, A.; Thelakkat, M.; Krausch, G. Charge Separation at Self-Assembled Nanostructured Bulk Interface in Block Copolymers. *Angew. Chem. Int. Ed.* **2006**, *45* (20), 3364–3368.

(32) Zhang, Q.; Cirpan, A.; Russell, T. P.; Emrick, T. Donor−Acceptor Poly(thiophene- *block* -Perylene Diimide) Copolymers: Synthesis and Solar Cell Fabrication. *Macromolecules* **2009**, *42* (4), 1079–1082.
(33) Tao, Y.; McCulloch, B.; Kim, S.; Segalman, R. A. The Relationship between Morphology and Performance of Donor–acceptor Rod–coil Block Copolymer Solar Cells. *Soft Matter* **2009**, *5* (21), 4219.
(34) Miyanishi, S.; Zhang, Y.; Tajima, K.; Hashimoto, K. Fullerene Attached All-Semiconducting Diblock Copolymers for Stable Single-Component Polymer Solar Cells. *Chem. Commun.* **2010**, *46* (36), 6723.
(35) Stalmach, U.; de Boer, B.; Videlot, C.; van Hutten, P. F.; Hadziioannou, G. Semiconducting Diblock Copolymers Synthesized by Means of Controlled Radical Polymerization Techniques. *J. Am. Chem. Soc.* **2000**, *122* (23), 5464–5472.
(36) van der Veen, M. H.; de Boer, B.; Stalmach, U.; van de Wetering, K. I.; Hadziioannou, G. Donor−Acceptor Diblock Copolymers Based on PPV and C_{60}: Synthesis, Thermal Properties, and Morphology. *Macromolecules* **2004**, *37* (10), 3673–3684.
(37) Barrau, S.; Heiser, T.; Richard, F.; Brochon, C.; Ngov, C.; van de Wetering, K.; Hadziioannou, G.; Anokhin, D. V.; Ivanov, D. A. Self-Assembling of Novel Fullerene-Grafted Donor–Acceptor Rod−Coil Block Copolymers. *Macromolecules* **2008**, *41* (7), 2701–2710.
(38) Scherf, U.; Gutacker, A.; Koenen, N. All-Conjugated Block Copolymers. *Acc. Chem. Res.* **2008**, *41* (9), 1086–1097.
(39) Verduzco, R.; Botiz, I.; Pickel, D. L.; Kilbey, S. M.; Hong, K.; Dimasi, E.; Darling, S. B. Polythiophene- *block* -Polyfluorene and Polythiophene- *block* -Poly(fluorene- *co* -Benzothiadiazole): Insights into the Self-Assembly of All-Conjugated Block Copolymers. *Macromolecules* **2011**, *44* (3), 530–539.
(40) Willot, P.; Moerman, D.; Leclère, P.; Lazzaroni, R.; Baeten, Y.; Van der Auweraer, M.; Koeckelberghs, G. One-Pot Synthesis and Characterization of All-Conjugated Poly(3-Alkylthiophene)- *block* -poly(dialkylthieno[3,4- *b*]pyrazine). *Macromolecules* **2014**, *47* (19), 6671–6678.
(41) Wang, S.; Yang, Q.; Tao, Y.; Guo, Y.; Yang, J.; Liu, Y.; Zhao, L.; Xie, Z.; Huang, W. Fully Conjugated Block Copolymers for Single-Component Solar Cells: Synthesis, Purification, and Characterization. *New J Chem* **2016**, *40* (2), 1825–1833.
(42) Lin, Y.-H.; Yager, K. G.; Stewart, B.; Verduzco, R. Lamellar and Liquid Crystal Ordering in Solvent-Annealed All-Conjugated Block Copolymers. *Soft Matter* **2014**, *10* (21), 3817–3825.
(43) Lee, Y.-H.; Chen, W.-C.; Yang, Y.-L.; Chiang, C.-J.; Yokozawa, T.; Dai, C.-A. Co-Crystallization Phase Transformations in All π-Conjugated Block Copolymers with Different Main-Chain Moieties. *Nanoscale* **2014**, *6* (10), 5208.
(44) Bridges, C. R.; Yan, H.; Pollit, A. A.; Seferos, D. S. Controlled Synthesis of Fully π-Conjugated Donor–Acceptor Block Copolymers Using a Ni(II) Diimine Catalyst. *ACS Macro Lett.* **2014**, *3* (7), 671–674.
(45) Hwang, Y.-J.; Earmme, T.; Courtright, B. A. E.; Eberle, F. N.; Jenekhe, S. A. N-Type Semiconducting Naphthalene Diimide-Perylene Diimide Copolymers: Controlling Crystallinity, Blend Morphology, and Compatibility Toward High-Performance All-Polymer Solar Cells. *J. Am. Chem. Soc.* **2015**, *137* (13), 4424–4434.

(46) Smith, K. A.; Lin, Y.-H.; Mok, J. W.; Yager, K. G.; Strzalka, J.; Nie, W.; Mohite, A. D.; Verduzco, R. Molecular Origin of Photovoltaic Performance in Donor- *block* -Acceptor All-Conjugated Block Copolymers. *Macromolecules* **2015**, *48* (22), 8346–8353.
(47) Verswyvel, M.; Steverlynck, J.; Hadj Mohamed, S.; Trabelsi, M.; Champagne, B.; Koeckelberghs, G. All-Conjugated ABC- *block* -Copolymer Formation with a Varying Sequence via an Unassociated Catalyst. *Macromolecules* **2014**, *47* (14), 4668–4675.
(48) Tkachov, R.; Komber, H.; Rauch, S.; Lederer, A.; Oertel, U.; Häußler, L.; Voit, B.; Kiriy, A. One-Pot Synthesis of All-Conjugated Block-Like Bisthiophene–Naphthalenediimide/Fluorene Copolymer. *Macromolecules* **2014**, *47* (15), 4994–5001.
(49) Erdmann, T.; Back, J.; Tkachov, R.; Ruff, A.; Voit, B.; Ludwigs, S.; Kiriy, A. Dithienosilole-Based All-Conjugated Block Copolymers Synthesized by a Combination of Quasi-Living Kumada and Negishi Catalyst-Transfer Polycondensations. *Polym. Chem.* **2014**, *5* (18), 5383.
(50) Dattani, R.; Bannock, J. H.; Fei, Z.; MacKenzie, R. C. I.; Guilbert, A. A. Y.; Vezie, M. S.; Nelson, J.; de Mello, J. C.; Heeney, M.; Cabral, J. T.; Nedoma, A. J. A General Mechanism for Controlling Thin Film Structures in All-Conjugated Block Copolymer:fullerene Blends. *J. Mater. Chem. A* **2014**, *2* (35), 14711.
(51) Gao, D.; Hollinger, J.; Seferos, D. S. Selenophene–Thiophene Block Copolymer Solar Cells with Thermostable Nanostructures. *ACS Nano* **2012**, *6* (8), 7114–7121.
(52) Chen, X. L.; Jenekhe, S. A. Block Conjugated Copolymers: Toward Quantum-Well Nanostructures for Exploring Spatial Confinement Effects on Electronic, Optoelectronic, and Optical Phenomena. *Macromolecules* **1996**, *29* (19), 6189–6192.
(53) Wu, P.-T.; Ren, G.; Li, C.; Mezzenga, R.; Jenekhe, S. A. Crystalline Diblock Conjugated Copolymers: Synthesis, Self-Assembly, and Microphase Separation of Poly(3-Butylthiophene)- *b* -poly(3-Octylthiophene). *Macromolecules* **2009**, *42* (7), 2317–2320.
(54) Lombeck, F.; Komber, H.; Sepe, A.; Friend, R. H.; Sommer, M. Enhancing Phase Separation and Photovoltaic Performance of All-Conjugated Donor–Acceptor Block Copolymers with Semifluorinated Alkyl Side Chains. *Macromolecules* **2015**, *48* (21), 7851–7860.
(55) Guo, C.; Lin, Y.-H.; Witman, M. D.; Smith, K. A.; Wang, C.; Hexemer, A.; Strzalka, J.; Gomez, E. D.; Verduzco, R. Conjugated Block Copolymer Photovoltaics with near 3% Efficiency through Microphase Separation. *Nano Lett.* **2013**, *13* (6), 2957–2963.
(56) Earmme, T.; Hwang, Y.-J.; Murari, N. M.; Subramaniyan, S.; Jenekhe, S. A. All-Polymer Solar Cells with 3.3% Efficiency Based on Naphthalene Diimide-Selenophene Copolymer Acceptor. *J. Am. Chem. Soc.* **2013**, *135* (40), 14960–14963.
(57) Mu, C.; Liu, P.; Ma, W.; Jiang, K.; Zhao, J.; Zhang, K.; Chen, Z.; Wei, Z.; Yi, Y.; Wang, J.; Yang, S.; Huang, F.; Facchetti, A.; Ade, H.; Yan, H. High-Efficiency All-Polymer Solar Cells Based on a Pair of Crystalline Low-Bandgap Polymers. *Adv. Mater.* **2014**, *26* (42), 7224–7230.
(58) Huang, H.; Zhou, N.; Ortiz, R. P.; Chen, Z.; Loser, S.; Zhang, S.; Guo, X.; Casado, J.; López Navarrete, J. T.; Yu, X.; Facchetti, A.; Marks, T. J. Alkoxy-Functionalized Thienyl-Vinylene Polymers for Field-Effect Transistors and All-Polymer Solar Cells. *Adv. Funct. Mater.* **2014**, *24* (19), 2782–2793.
(59) Mok, J. W.; Lin, Y.-H.; Yager, K. G.; Mohite, A. D.; Nie, W.; Darling, S. B.; Lee, Y.; Gomez, E.; Gosztola, D.; Schaller, R. D.; Verduzco, R. Linking Group Influences Charge

Separation and Recombination in All-Conjugated Block Copolymer Photovoltaics. *Adv. Funct. Mater.* **2015**, *25* (35), 5578–5585.
(60) Botiz, I.; Schaller, R. D.; Verduzco, R.; Darling, S. B. Optoelectronic Properties and Charge Transfer in Donor–Acceptor All-Conjugated Diblock Copolymers. *J. Phys. Chem. C* **2011**, *115* (18), 9260–9266.
(61) Johnson, K.; Huang, Y.-S.; Huettner, S.; Sommer, M.; Brinkmann, M.; Mulherin, R.; Niedzialek, D.; Beljonne, D.; Clark, J.; Huck, W. T. S.; Friend, R. H. Control of Intrachain Charge Transfer in Model Systems for Block Copolymer Photovoltaic Materials. *J. Am. Chem. Soc.* **2013**, *135* (13), 5074–5083.
(62) Ma, W.; Tumbleston, J. R.; Wang, M.; Gann, E.; Huang, F.; Ade, H. Domain Purity, Miscibility, and Molecular Orientation at Donor/Acceptor Interfaces in High Performance Organic Solar Cells: Paths to Further Improvement. *Adv. Energy Mater.* **2013**, *3* (7), 864–872.
(63) Burke, T. M.; McGehee, M. D. How High Local Charge Carrier Mobility and an Energy Cascade in a Three-Phase Bulk Heterojunction Enable >90% Quantum Efficiency. *Adv. Mater.* **2014**, *26*, 1923-1928.
(64) Wienk, M. M.; Turbiez, M.; Gilot, J.; Janssen, R. A. J. Narrow-Bandgap Diketo-Pyrrolo-Pyrrole Polymer Solar Cells: The Effect of Processing on the Performance. *Adv. Mater.* **2008**, *20* (13), 2556–2560.
(65) Li, W.; Roelofs, W. S. C.; Turbiez, M.; Wienk, M. M.; Janssen, R. A. J. Polymer Solar Cells with Diketopyrrolopyrrole Conjugated Polymers as the Electron Donor and Electron Acceptor. *Adv. Mater.* **2014**, *26* (20), 3304–3309.
(66) Zhang, X.; Richter, L. J.; DeLongchamp, D. M.; Kline, R. J.; Hammond, M. R.; McCulloch, I.; Heeney, M.; Ashraf, R. S.; Smith, J. N.; Anthopoulos, T. D.; Schroeder, B.; Geerts, Y. H.; Fischer, D. A.; Toney, M. F. Molecular Packing of High-Mobility Diketo Pyrrolo-Pyrrole Polymer Semiconductors with Branched Alkyl Side Chains. *J. Am. Chem. Soc.* **2011**, *133* (38), 15073–15084.
(67) McCulloch, B.; Ho, V.; Hoarfrost, M.; Stanley, C.; Do, C.; Heller, W. T.; Segalman, R. A. Polymer Chain Shape of Poly(3-Alkylthiophenes) in Solution Using Small-Angle Neutron Scattering. *Macromolecules* **2013**, *46* (5), 1899–1907.
(68) Schmidt, K.; Tassone, C. J.; Niskala, J. R.; Yiu, A. T.; Lee, O. P.; Weiss, T. M.; Wang, C.; Fréchet, J. M. J.; Beaujuge, P. M.; Toney, M. F. A Mechanistic Understanding of Processing Additive-Induced Efficiency Enhancement in Bulk Heterojunction Organic Solar Cells. *Adv. Mater.* **2014**, *26* (2), 300–305.
(69) Kim, J. Y.; Frisbie, C. D. Correlation of Phase Behavior and Charge Transport in Conjugated Polymer/Fullerene Blends. *J. Phys. Chem. C* **2008**, *112* (45), 17726–17736.
(70) Verploegen, E.; Mondal, R.; Bettinger, C. J.; Sok, S.; Toney, M. F.; Bao, Z. Effects of Thermal Annealing Upon the Morphology of Polymer–Fullerene Blends. *Adv. Funct. Mater.* **2010**, *20* (20), 3519–3529.
(71) Khlyabich, P. P.; Rudenko, A. E.; Thompson, B. C.; Loo, Y.-L. Structural Origins for Tunable Open-Circuit Voltage in Ternary-Blend Organic Solar Cells. *Adv. Funct. Mater.* **2015**, *25* (34), 5557–5563.
(72) Kline, R. J.; McGehee, M. D.; Kadnikova, E. N.; Liu, J.; Fréchet, J. M. J.; Toney, M. F. Dependence of Regioregular Poly(3-Hexylthiophene) Film Morphology and Field-Effect Mobility on Molecular Weight. *Macromolecules* **2005**, *38* (8), 3312–3319.

(73) Zhang, R.; Li, B.; Iovu, M. C.; Jeffries-EL, M.; Sauvé, G.; Cooper, J.; Jia, S.; Tristram-Nagle, S.; Smilgies, D. M.; Lambeth, D. N.; McCullough, R. D.; Kowalewski, T. Nanostructure Dependence of Field-Effect Mobility in Regioregular Poly(3-Hexylthiophene) Thin Film Field Effect Transistors. *J. Am. Chem. Soc.* **2006**, *128* (11), 3480–3481.
(74) Wang, C.; Lee, D. H.; Hexemer, A.; Kim, M. I.; Zhao, W.; Hasegawa, H.; Ade, H.; Russell, T. P. Defining the Nanostructured Morphology of Triblock Copolymers Using Resonant Soft X-Ray Scattering. *Nano Lett.* **2011**, *11* (9), 3906–3911.
(75) Guo, C.; Kozub, D. R.; Vajjala Kesava, S.; Wang, C.; Hexemer, A.; Gomez, E. D. Signatures of Multiphase Formation in the Active Layer of Organic Solar Cells from Resonant Soft X-Ray Scattering. *ACS Macro Lett.* **2013**, *2* (3), 185–189.
(76) Virgili, J. M.; Tao, Y.; Kortright, J. B.; Balsara, N. P.; Segalman, R. A. Analysis of Order Formation in Block Copolymer Thin Films Using Resonant Soft X-Ray Scattering. *Macromolecules* **2007**, *40* (6), 2092–2099.
(77) Liu, J.; Loewe, R. S.; McCullough, R. D. Employing MALDI-MS on Poly(alkylthiophenes): Analysis of Molecular Weights, Molecular Weight Distributions, End-Group Structures, and End-Group Modifications. *Macromolecules* **1999**, *32* (18), 5777–5785.
(78) Smith, K. A.; Pickel, D. L.; Yager, K.; Kisslinger, K.; Verduzco, R. Conjugated Block Copolymers via Functionalized Initiators and Click Chemistry. *J. Polym. Sci. Part Polym. Chem.* **2014**, *52* (2), 154–163.

Table of Contents Graphic